

Chemisorption of CO₂ in A Gas-Liquid Vortex Reactor: An Interphase Mass Transfer Efficiency Assessment

Yi Ouyang, Manuel Nunez Manzano, Siyuan Chen, Ruben Wetzels, Tom Verspeelt,

Kevin M. Van Geem, Geraldine J. Heynderickx*

Ghent University, Laboratory for Chemical Technology, Technologiepark 125, 9052 Gent,
Belgium.

*Corresponding author:

Kevin M. Van Geem

Laboratory for Chemical Technology, Ghent University, Belgium

Address: Technologiepark 125, B-9052 Ghent, Belgium

Tel. : +32 9 264 56 77 /Fax: +32 9 331 1759

Kevin.VanGeem@UGent.be

This article has been accepted for publication and undergone full peer review but has not been through the copyediting, typesetting, pagination and proofreading process which may lead to differences between this version and the [Version of Record](#). Please cite this article as doi: [10.1002/aic.17608](https://doi.org/10.1002/aic.17608) © 2022 American Institute of Chemical Engineers
Received: Aug 18, 2021; Revised: Jan 05, 2022; Accepted: Jan 15, 2022

This article is protected by copyright. All rights reserved.

Accepted Article

Highlights

1. A gas-liquid vortex reactor is assessed for process intensification of interphase mass transfer.
2. The highly turbulent gas-liquid contact in the reactor generates a large specific interfacial area and significantly intensifies interphase mass transfer.
3. A superior mass transfer efficiency is achieved with a favorable energetic efficiency.

Keywords: Gas-Liquid Vortex Reactor; Interphase Mass Transfer; Process Intensification; CO₂ Capture

Abstract

To develop cost-effective CO₂ capture technology process intensification will play a vital role. In this work the capabilities of a gas-liquid vortex reactor (GLVR) as novel process intensification equipment are evaluated by studying its interphase mass transfer parameters to build up the fundamentals for its future application to e.g. CO₂ capture. The NaOH-CO₂ chemisorption system and Danckwerts' model are applied to obtain the effective interfacial area and liquid-side mass transfer coefficient. Results show that the gas-liquid contact in the GLVR is capable of both generating a large interfacial area in a small reactor volume and creating a region with high energy dissipation to improve mass transfer. A comparison of the volumetric mass transfer coefficients with data reported in literature for conventional and intensified reactor types confirms a superior mass transfer efficiency and, most importantly, a favorable energetic efficiency of the GLVR.

Introduction

The state-of-the-art technologies for CO₂ capture are characterized by high OPEX and CAPEX mainly due to significant energy requirements for solvent regeneration and large column sizes respectively^{1,2}. In view of reducing OPEX, a lot of past research has focused on the development of new solvent types with low heats of absorption, as these are associated with lower thermal energy requirements in the solvent regeneration step³⁻⁷. Depending on the exact operating conditions, the type of solvent used can possibly also influence the CAPEX of the CO₂ scrubbing equipment, as it influences the sorption rate at high solvent concentrations⁸. However, there is another path to tackle the above challenges in the CO₂ capture industry, namely by developing process intensification equipment/methods to increase the energy efficiency and decrease the capital cost^{2,9}. Examples include the application of rotating packed bed¹⁰⁻¹², microreactor¹³⁻¹⁶ and other intensified equipment^{17,18}.

Absorption of CO₂ in solvents is mostly based on the physical transfer of CO₂ between a gas and liquid phase, combined with a reversible, liquid side neutralization reaction of CO₂ with the sorbent. As such, there are two limiting factors affecting the CO₂ absorption in view of the transport process: the interphase mass transfer of CO₂ and the mixing-reaction process at the liquid side. The latter is sometimes referred to as the micromixing process¹⁹. As the CO₂-solvent reaction is in most cases categorized as a fast reaction, mass transfer through the liquid film near the gas-liquid interface is the limiting phenomenon for the overall absorption performance^{2,20}, especially when the mixing-reaction process is rather quick compared to the interphase mass transfer. Improving the interphase mass transfer efficiency is thus of primary importance when developing new process intensification equipment and methods. Through reactor design one can influence the fundamental interphase mass transfer parameters, being

the effective specific interfacial area and the liquid-side mass transfer coefficient, to effectively increase the volumetric absorption rate ⁸.

A gas-liquid vortex reactor (GLVR) is expected to fulfill these needs for process intensification as most recent studies have confirmed its promising potential in terms of gas-liquid hydrodynamics ²¹ and micromixing efficiency at the liquid side ²². The GLVR is a cylinder-shaped, static fluidization chamber in which gas is tangentially injected through multiple gas inlet slots in the outer cylindrical wall, while the liquid is introduced in a co-current contacting way with the gas flow as shown *Figure 1*. Without mechanical rotation, a rotating gas-liquid layer is formed in the vortex chamber under continuous operation. The balance between the radially inward gas drag force and radially outward centrifugal force holds a certain amount of liquid near the outer edge of the vortex chamber, constantly refreshing the liquid into a dynamic equilibrium state and generating a large gas-liquid interfacial area ²¹. It is worth mentioning that previous studies mainly focused on the vortex reactor used in gas-solid systems ^{23–34}. Successful experience has led to the exploration of gas-liquid systems in the reactor, and more specifically of CO₂ capture in this study. However, prior to practical applications, the interphase mass transfer efficiency of the GLVR should be evaluated to justify the potential of the GLVR for processes limited by interphase mass transfer, such as CO₂ capture ¹⁰, H₂S absorption ³⁵, volatile organic compounds removal ³⁶, etc.

Figure 1 Schematic of the gas-liquid vortex reactor: (a) top view, (b) side view ²²

In general, for an interphase mass transfer study knowledge of the effective interfacial area is of major importance as it will further affect the evaluation of the mass transfer coefficient ³⁷. Experimental approaches to determine the effective interfacial area mainly include physical methods, e.g. high-speed imaging ^{38,39}, tomography ^{40,41} and colorimetry ⁴², and chemical methods, e.g. chemisorption of O₂ using aqueous Na₂SO₃ ⁴³ and chemisorption of CO₂ using

aqueous NaOH as the most adopted ones^{37,44}. It should be noted that in the case of a NaOH-CO₂ system for example, there are various combinations of kinetic models and models to calculate the Henry's law coefficient and diffusivity coefficient, resulting in absolute value deviations in the final calculated effective interfacial area⁴⁵. This is also the case when determining the mass transfer coefficient⁴³, or to be more specific, the liquid-side mass transfer coefficient in this study, as CO₂ absorption is a typical process controlled by the liquid-side resistance^{37,46,47}.

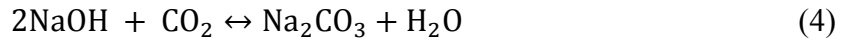
This work aims to provide fundamental data of the gas-liquid mass transfer parameters that can be used to assess the efficiency of the GLVR. Via chemisorption of NaOH-CO₂, the effective specific interfacial area (a_e) and the liquid-side mass transfer coefficient (k_L) of the GLVR are determined by Danckwerts' model as explained in detail below. The operating window of the GLVR is discussed. A benchmark assessment of the GLVR is given based on the liquid-side volumetric mass transfer coefficient.

Model

NaOH-CO₂ reaction system

Given the advantages of well-defined kinetics, liquid-side controlled absorption, availability in literature of detailed models and convenience of experimental work⁴⁵, the NaOH-CO₂ chemisorption is adopted in this study. Eqs. 1 to 3 show the reaction steps associated with CO₂ absorption into an aqueous NaOH solution⁴⁵. Eq. 4 is the global reaction equation for the reaction between NaOH and CO₂.





Reaction 1 is the dissolution step of gas phase CO₂. The liquid-side concentration of CO₂ at the interface C_{CO_2} can be obtained from Henry's law:

$$C_{\text{CO}_2} = \frac{P_{\text{CO}_2}}{H_{e\text{CO}_2}} \quad (5)$$

where $H_{e\text{CO}_2}$ is Henry's law volatility constant (Pa·m³/mol) of CO₂ in the NaOH solution and P_{CO_2} is the gas bulk CO₂ partial pressure. To be specific, P_{CO_2} is determined by the logarithmic mean of the CO₂ partial pressure at the reactor inlet and outlet^{45,48}. Reaction 2 is the reaction between dissolved CO₂ and a hydroxyl ion to form bicarbonate, which is the rate-determining step in the reaction mechanism sequence. Reaction 3 is the final step, where the bicarbonate reacts with a second hydroxyl ion to produce carbonate and water. It is a proton transfer reaction that can be considered as instantaneous. As reaction 2 is the rate-determining step, the overall reaction rate can be expressed as:

$$R_r = k_{\text{OH}} C_{\text{OH}} C_{\text{CO}_2} \quad (6)$$

where k_{OH} is the rate constant and C_{OH} and C_{CO_2} are the concentration of hydroxyl ions and CO₂ respectively. If the reaction occurs in a large excess of NaOH, pseudo first-order kinetics is valid and the first-order rate constant can be defined as:

$$k_1 = k_{\text{OH}} C_{\text{OH}} \quad (7)$$

From an experimental point of view, C_{OH} can be determined from the average concentration of the hydroxide ion measured at the inlet and outlet. The key is thus to model the k_{OH} as it is a function of temperature and ionic strength. Sheng et al.⁴⁵ reviewed different sources of kinetic models and physical properties and concluded that the parameter source developed by Phorecki and Moniuk⁴⁹ is the recommended one to use for the calculation of mass transfer characteristics

from absorption measurements. It includes a kinetic model for the rate constant k_{OH} , as well as correlations to calculate physical properties such as D_{CO_2} and for the Henry's law constant of CO_2 in the NaOH solution (He_{CO_2}). The model is often considered as one of the most representative models, with its results often used as reference data ⁴⁵, which is also the main reason why it is adopted in this work.

Danckwerts' model

The model used in this work is based on Danckwerts' model ⁴⁴ and is summarized in a recent review ³⁷. Danckwerts' method proposed in 1970 has been widely used in mass transfer studies to obtain values for a_e and k_L from experimental absorption measurements ^{37,50–54}. The method is based on the surface renewal theory, in which a parameter s is introduced representing the renewal rate of the liquid surface, i.e. the fraction of surface area replaced with fresh fluid per unit of time ^{8,55}. It is proposed that the exposure time of the liquid elements in the renewed surface follows a surface-age distribution function of an exponential form. In Danckwerts' mass transfer model, the rate of absorption into the liquid is expressed as the average value of the flux over all liquid elements at the surface (N_A), given by Eq. 8:

$$N_A = \int_0^{\infty} s N_i e^{-st} dt \quad (8)$$

Using a Laplace transformation on the governing partial differential equation (Fick's second law) and using the proper boundary conditions, Danckwerts derived the following expression for the volumetric absorption rate R_{CO_2} (mol/(m³·s)), as a function of variables that can be measured or modelled:

$$R_{CO_2} = k_L a_e C_{CO_2} E \quad (9)$$

E is defined as the enhancement factor, i.e. the ratio of mass transfer coefficient with and without chemical reaction.

Further discussion needs a dimensionless number, the Hatta number (*Ha*), as defined in Eq. 10 for a (pseudo) first-order reaction:

$$Ha = \frac{\sqrt{D_{CO_2}k_1}}{k_L} \quad (10)$$

where D_{CO_2} is the diffusivity coefficient of CO₂ in the NaOH solution.

Using the above equations, **Figure 2** shows the calculation procedure to determine the effective specific interfacial area a_e , liquid side mass-transfer coefficient k_L , and volumetric liquid-side mass transfer coefficient k_La_e . The procedure can be divided into three steps:

(1) Eq.12 in **Figure 2** corresponds to Eq. 9 but the absorption rate is expressed by molar absorption rate \dot{n}_{CO_2} (mol/s), while A_e is the total effective interfacial area. The absorption rate \dot{n}_{CO_2} is given by:

$$\dot{n}_{CO_2} = L\Delta C_{CO_3^{2-}} \quad (11)$$

where L is the liquid flow rate and $\Delta C_{CO_3^{2-}}$ is the concentration difference of Na₂CO₃ at the reactor inlet and outlet. As the inlet liquid stream only contains NaOH, a measurement of the outlet Na₂CO₃ concentration allows a determination of $\Delta C_{CO_3^{2-}}$.

If the constraint $Ha > 3$ is fulfilled (or $Ha > 2$ or $Ha > 5$ in some studies³⁷), the enhancement factor E can be approximated as equal to Ha and Eq.12 in **Figure 2** can be simplified into Eq.13. As such, A_e can be directly obtained from the absorption experiment as the k_L term can be neglected. a_e can be further determined by dividing A_e by the reactor volume (or by dividing the packing volume in some studies⁵⁰). To be specific, the reactor volume is determined by the volume of the whole reactor chamber in this study. To achieve a $Ha > 3$, a relatively high

concentration NaOH solution is needed for the a_e experiments, such as 1.25 M NaOH as used in this work. As a result, the gas phase CO₂ concentration also needs to be properly chosen: if the CO₂ concentration is too high, the NaOH concentration difference between the liquid inlet and outlet of the reactor will vary too much, which increases the model error when calculating the average C_{OH} ; if the CO₂ concentration is too low, the NaOH concentration difference becomes lower which increases the experimental measurement error. Therefore a CO₂ concentration of 10 vol % is adopted in this work.

(2) After obtaining the A_e values under various operating conditions, A_e can be used to calculate k_L . If $Ha < 1$, the approximation of $E = \sqrt{1 + Ha^2}$ can be used based on Danckwerts' Plot³⁷. To achieve a $Ha < 1$, a relatively low concentration NaOH solution is needed, such as 0.1 M NaOH shown in **Figure 2**. Based on the same considerations as for the first experiment to obtain the A_e values, a CO₂ concentration of 2.5 vol% is selected for the experiments to obtain k_L . Note that the A_e value obtained from Eq. 13 is not strictly equal to the value in Eq. 15, as a different NaOH concentration is used. However, the main factor affecting the interfacial area is the operating conditions⁵², i.e. the gas flow rate and liquid flow rate in this study. Therefore, under the same operating conditions, the A_e values obtained from the Eq.13 can be used in Eq.15.

(3) Only if k_L is known, one can calculate the corresponding Ha number. Therefore, validation is needed to check if the two constraints are met, i.e. $Ha > 3$ in the a_e experiment in step 1 and $Ha < 1$ in the k_L experiment in step 2. The volumetric liquid-side mass transfer coefficient $k_L a_e$ is the product of k_L and a_e , which can be used to benchmark the reactor's performance³⁹. 12
13 14 15 16,)

Figure 2 Schematic overview of the models to determine effective specific interfacial area a_e , liquid-side mass transfer coefficient k_L , and volumetric liquid-side mass transfer coefficient k_{LA_e} .

Experimental procedures

Gas-liquid vortex reactor setup

Figure 3 shows a schematic overview of the experimental setup. Apart from the GLVR itself, a liquid feeding section, a gas feeding section and a sampling & analysis section can be identified. The liquid feeding section includes a NaOH storage tank which contains a prepared NaOH solution of either 1.25 or 0.1 M, depending on the experiment. A high precision gear pump (Tuthill DGS1.2) with a flow meter (Cori-Flow M55) withdraws the NaOH solution from the storage tank and pumps it into the GLVR via a single liquid inlet pipe through the upper reactor end wall. The gas feeding section includes both the N₂ and CO₂ storage cylinders, as well as two control valves to adjust the flow rate and CO₂ concentration. The N₂-CO₂ mixture flows through the gas feeding line, into the annular jacket surrounding the vortex chamber. From this jacket, the gas mixture enters the reactor zone through 12 tangentially inclined inlet slots, circumferentially spaced over the outer wall of the vortex chamber of the GLVR to ensure a uniform gas distribution. The gas mixture that is tangentially injected into the vortex chamber transfers part of its momentum to the liquid phase thus creating a highly turbulent and dispersed gas-liquid mixture in a strong centrifugal field. The diverging exhaust, located in the center of the upper end wall, serves as the outlet for both the gas and liquid phase. Two cyclones in series are connected to the outlet of the GLVR to separate the gas and the liquid.

Table 1 provides dimensional information of the GLVR. The diameter of the cylindrical vortex chamber is 80 mm and the chamber has a height of 15 mm. The exhaust above the vortex

chamber has a diameter of 20 mm at the throat and diverges to a maximum diameter of 60 mm near the outlet, shown in the GLVR front view in **Figure 3**. The 12 inlet slots in the GLVR used in this study have a width of 0.65 mm and are inclined at an angle of 10° with respect to a tangent line to the vortex chamber. The liquid inlet pipe has a diameter of 4 mm and is positioned at an angle of 18° with respect to the upper end wall of the GLVR. When the gas and liquid are introduced in the GLVR and reach a steady state, a gas-liquid layer will be formed near the out wall of the vortex chamber. The gas-liquid layer thickness (L_t) is shown in **Figure 3** in the GLVR front view.

Figure 3 Schematic view of the gas-liquid vortex reactor setup for the NaOH-CO₂ chemisorption experiments.

Table 1 Geometrical parameters of the GLVR.

Sampling and analysis

To calculate the rate of CO₂ interphase mass transfer, both the liquid and the gas phase exiting the GLVR are measured on their CO₂ content. (1) For the liquid side, a four-electrode conductivity probe (METTLER TOLEDO Transmitter M200) is used for online and fast measurement of the amount of CO₂ absorbed into NaOH solutions. Similar approaches have been used by several authors to measure the liquid side absorbed CO₂ in a continuous way^{56,57}. The method is based on the fact that absorbed CO₂ reacts to carbonate (CO_3^{2-}) (Eq. 4) and the result of this is that the conductivity of the NaOH solution significantly drops while absorbing CO₂. To use this measurement method, a calibration curve is made by measuring the liquid conductivity of solutions containing varying proportions of NaOH and Na₂CO₃ of equal molarity. It was observed by Bayliss⁵⁸ that such a calibration curve, plotting the conductivity as a function of the carbonate fraction, is linear, making it easy to deduct carbonate

concentrations from continuous conductivity measurements. (2) For the gas side CO₂ analysis, an online IR analyser (Fuji Infrared Gas Analyzer) is used to detect the CO₂ percentage.

As can be seen from the sampling & analysis section shown in **Figure 3**, a separate sampling line is provided for both phases. The use of a single sampling line to simultaneously extract both phases from the GLVR, to then analyse both phases separately after phase separation, results in great error. This error is attributed to the fact that the gas-liquid contact time in the sampling line would be higher than the gas-liquid contact time in the GLVR itself, causing the absorption process to proceed in the sampling line to an extent that cannot be neglected. In general, it should be avoided that the gas is sampled with too much liquid and vice versa.

As the liquid is the heavier phase that is likely to attach to the reactor wall, the gas sampling point is located at the center of the throat and the liquid sampling point at the throat wall, as shown in **Figure 3**. Using this approach, the gas-liquid volumetric ratio (R) in the sampling lines is significantly reduced or increased compared to the R of 100-700 in the GLVR. Using the liquid sampling setup depicted in **Figure 3**, the R value in the liquid sampling line can be determined. The vacuum pump withdraws a continuous flow of gas from the liquid sample container, while the liquid itself is collected in the container. By reading the liquid level in the liquid sample container after a given time, the R value can be calculated, which is found to be around 2-3. By theoretically calculating the maximum amount of supplementary CO₂ absorption that can occur in the liquid sampling pipe, the maximum attainable deviation of the measured liquid NaOH concentration from the true outlet NaOH concentration is found to be ~3% for an R value of 3 in the liquid sampling line. Similarly, when performing the experiments, the vacuum pump in the liquid sampling line in **Figure 3** withdraws the continuous flow of gas from the liquid sample container. The red part in the sensor vessel is the conductivity probe and can give the online measurement of the liquid conductivity. Such

Accepted Article

configuration makes the liquid sample stream easily submerge the probe. The sensor vessel works like communicating vessels, with the liquid being withdrawn both from the top and bottom of the liquid volume. As such, it is ensured the liquid is constantly being updated for the probe reading.

The gas is sampled by a vacuum pump at a low flow rate (0.5 ± 0.05 L/min) from a central point at the throat where the gas holdup is dominant. This gas sampling location ensures that the gas is sampled without a significant amount of liquid being sucked out of the reactor. A verification is done similar to the liquid sampling line and the maximum attainable deviation is ~5%. After passing two drying elements filled with Drierite to ensure proper removal of water vapor, the gas mixture flows through a rotameter to measure and control the gas flow being sent to the IR analyser.

As the CO₂ removed from the gas side and CO₂ absorbed by the liquid side can both be calculated, a comparison can be made based on the CO₂ removal rate at the gas side and CO₂ absorbed rate at the liquid side to justify the analysis in this study. This comparison has been made for all data points in this work and on average the gas side removed CO₂ and liquid side absorbed CO₂ show a good agreement. As the liquid flow controller and online measurement of the liquid side CO₂ content show a more steady signal during the experiment, the liquid side data is used to determine the molar absorption rate of CO₂ as shown in Eq. 11. The latter is a common practice in literature ⁴⁵.

Next to the liquid and gas sampling lines, pressure and temperature probes are also installed in the GLVR at the locations depicted in *Figure 3*. The first measurement point for pressure is located near the intersection point of the top end wall and the outer wall of the vortex chamber. The second measurement point both for pressure and temperature is positioned near the throat of the central exhaust. Using the difference between both pressure readings, the pressure drop

across the gas-liquid layer in the vortex chamber can be calculated. In addition, the CO₂ partial pressure can also be calculated combined with the IR analyser.

Experimental procedure

For each combination of gas and liquid flow rates, the general experimental procedure can be summarized as follows. (1) Firstly, an experiment is performed at high NaOH concentration (1.25 M) and high CO₂ concentration (10 vol%) to ensure that $Ha > 3$. As such, the total effective interfacial area A_e can be determined as described above. (2) Subsequently, the experiment is repeated with the same gas and liquid flow rates, such that the hydrodynamics remain largely unaltered, but at low NaOH concentration (0.1 M) and low CO₂ concentration (2.5 vol%). Under these conditions, $Ha < 1$ and k_L can be obtained using the A_e value. (3) A post validation is done to ensure that the conditions of $Ha > 3$ and $Ha < 1$ are met. If the conditions are not met the experiments need to be rerun with a redetermined NaOH concentration and CO₂ concentration.

To calculate the molar absorption rate of CO₂, the key is to accurately measure the inlet and outlet concentration both at the liquid side, i.e. NaOH concentrations, and at the gas side, i.e. CO₂ concentrations, in addition to flow rates. The NaOH solution is prepared manually in batches of approximately 100 kg each to ensure the continuity and stability of the liquid feeding system. In addition, the conductivity of each prepared batch is measured by injecting the NaOH solution into the GLVR which is fed by a N₂-only gas phase, to avoid the conversion of hydroxyl ions into carbonate. The conductivity readings from the liquid samples during these N₂-only experiments are used as the inlet conductivities during data-processing. Every absorption experiment is started by specifying a set value for the CO₂ inlet concentration, and then introducing the gas phase N₂-CO₂ mixture into the GLVR, without any solvent being injected. In this gas-only operation, the inlet CO₂ concentration of the N₂-CO₂ mixture can be

measured by the IR analyser connected to the gas sampling line. The IR CO₂ concentration reading slightly lags behind the concentration value displayed by the input valve controller. Therefore, the steady state can be identified when both concentration readings match. At this moment, the liquid NaOH solution is introduced in the GLVR at the desired flow rate and molarity. After several minutes, a steady state is reached once again. The outlet CO₂ concentration in the gas phase and the outlet NaOH concentration in the liquid phase are measured by time-averaging both online readings over at least 30 seconds of measurement time.

Results and discussion

Pressure drop

Prior to studying the interphase mass transfer parameters, the role of gas phase and pressure drop in the GLVR should be discussed as this will form the basis for the mass transfer assessment. The gas phase in the GLVR is not only the gas feed but also the main energy input to the reactor. For a more detailed discussion reference is made to our previous work²¹: in the same GLVR geometry as used in this study, the gas-liquid flow patterns were revealed by high-speed imaging, indicating that a rotating gas-liquid layer is formed near the outer edge of the vortex chamber due to the balance between the radially inward gas drag force and radially outward centrifugal force. **Figure 4** shows the pressure drop over the GLVR for various combinations of gas flow rates and liquid flow rates. It can be observed that ΔP increases both with increasing liquid and gas flow rates. Overall, the influence of the gas flow rate on ΔP is higher than the influence of the liquid flow rate. When the vortex reactor was used for a gas-solid system, Pantzali et al.⁵⁹ measured the radial pressure profile of the vortex reactor and observed that most of the pressure drop in the vortex chamber occurs in the particle bed formed near the wall of the vortex chamber. This pressure drop was a main consequence of the gas-

Accepted Article

solid drag force in the particle bed, a measure for the ‘weight’ of the bed in the centrifugal field, being the dominant contribution. This reasoning is most likely still valid for the GLVR. On the one hand, increasing the gas flow rate will increase the gas drag force and increase the momentum transfer from the gas phase to the liquid phase in the rotating gas-liquid layer, resulting in a higher pressure drop. On the other hand, increasing the liquid flow rate will increase liquid holdup and the gas-liquid layer thickness in the GLVR ²¹. A higher liquid holdup implies that the radially inward flowing gas passes more liquid volume elements, driving more liquid into a rotational motion and consumes more gas momentum energy. A larger interfacial area is thus likely to be created. As the gas flow is the main energy input into the reactor, the overall energetic efficiency can be evaluated based on the pressure drop, as discussed in the subsequent sections.

Figure 4 Pressure drop over gas-liquid layer in the GLVR for various gas and liquid flow rates.

Effective specific interfacial area

Figure 5 shows the effect of the gas and liquid flow rate on the effective specific interfacial area a_e . a_e varies from 860 to up to 2750 m^2/m^3 depending on the gas and liquid flow rates to the reactor. It can be observed that an increase in the gas flow rate results in an increase in a_e for all values of the liquid flow rate. An increase in the liquid flow rate causes an initial increase in a_e for all gas flow rates up till a liquid flow rate of ~110-130 kg/h. At higher liquid flow rates, a_e starts to plateau. The influence of the gas flow rate on a_e is considerably higher than the influence of the liquid flow rate. In a previous study on the same GLVR geometry, a decrease in bubble size was observed with increasing gas flow rates in an air-water system ²¹. This is likely to happen as well in this study because with increasing gas flow rates more energy is introduced into the system, which explains the effect of gas flow rate on the interfacial area.

On the other hand, the effect of liquid flow rate can be explained by the change in the gas-liquid layer thickness as observed in the previous study ²¹, where a correlation was proposed to calculate this thickness:

$$L_t = -6.75 \log\left(\frac{G}{L}\right) + 49.8 \quad (17)$$

In Eq. 17, L_t is the gas-liquid layer thickness (mm) as shown in **Figure 3**, G is the gas flow rate (m^3/s) and L is the liquid volumetric flow rate (m^3/s). With a fixed gas flow rate G_0 , Eq. 17 can be reformulated as:

$$L_t = 6.75 \log(L) + 49.8 - \log(G_0) \quad (18)$$

From Eq. 18 it can be concluded that for a fixed gas flow rate the gas-liquid layer thickness will logarithmically increase with increasing liquid flow rate. As the increase in gas-liquid layer thickness will likely generate a larger interfacial area, the effect of the liquid flow rate on a_e in **Figure 5** is in line with the effect of the liquid flow rate on the gas-liquid layer thickness in Eq. 18, i.e. the increasing trend in a_e levels off when increasing the liquid flow rate. From Eq. 18 it should also be noted that increasing the gas flow rates G_0 will decrease the gas-liquid layer thickness, which seems to be not conducive to increasing the a_e . However, the dominating factor when changing the gas flow rate should be the change in bubble size rather than the formed gas-liquid layer thickness. As discussed above, smaller bubbles are formed with higher gas flow rates, and this dictates the effect of the gas flow rate on a_e .

There is another possible explanation for the plateau in the a_e profile under liquid flow rates higher than 110-120 kg/h. As the liquid holdup volume is likely to increase when increasing the liquid flow rate, the gas holdup volume will then decrease due to the fixed reactor volume. As a result, the gas mean residence time becomes too short to further enhance the gas dispersion and increase a_e . As such, the liquid flow rate should be limited to 110-130 kg/h in this study

(*Figure 5*), which also gives an indication of a proper operating window for practical application of the GLVR.

Figure 5 Effective specific interfacial area in the GLVR for various gas and liquid flow rates.

Liquid-side mass transfer coefficient

Figure 6 shows the effect of the gas and liquid flow rate on the liquid-side mass transfer coefficients k_L . At constant gas flow rate, k_L shows in general a slightly increasing trend with increasing liquid flow rate. At constant liquid flow rate, a sharp increase in k_L value is observed with increasing gas flow rate over the whole range of liquid flow rates. For the given change in liquid or gas flow rate, the effect on k_L is much larger for the gas flow rate than for the liquid flow rate. The underlying turbulent quantity explaining the influence of the gas and liquid flow rate on k_L is the turbulent kinetic energy dissipation rate. According to the eddy cell model⁶⁰, k_L is dependent on the turbulent dissipation rate. The strong gas flow in the GLVR induces a highly turbulent flow condition in the vortex chamber and increasing the gas or liquid flow rate will increase the turbulent dissipation. A previous study has shown that the gas flow rate is the dominant factor affecting the turbulent dissipation rate compared to the effect of the liquid flow rate²¹. In this previous study, the k_L was found to be in the range of 1×10^{-3} - 2×10^{-3} m/s based on the eddy cell model and turbulent dissipation rates determined from experimentally observed turbulent properties. A more rigorous way to determine the k_L , based on NaOH-CO₂ chemisorption, is given in this study, showing a reasonable agreement as shown from the values presented in *Figure 6*.

Figure 6 Liquid-side mass transfer coefficient in the GLVR for various gas flow and liquid flow rates.

Assessment of the GLVR performance

Comparison of effective specific interfacial area

In **Figure 7** the performance of the GLVR is compared to other gas-liquid reactors studied in literature based on the reported ranges for a_e . It should be noted that not all studies referred to in **Figure 7** made use of the same gas and liquid phase species. However, as changes in the physical properties of the gas and liquid used in literature have a limited effect on the a_e , a qualitative comparison based on the reported ranges is justifiable. From **Figure 7**, one can observe that in terms of the effective specific interfacial area range the GLVR outperforms several other types of gas-liquid reactors, which is a direct proof that the vortex type gas-liquid contact in the GLVR is capable of generating a large interfacial area in a relatively small volume. The comparison based on a_e shows that the GLVR outperforms typical conventional reactors by a factor 10 and other intensified reactor types (e.g. rotating packed bed) by a factor 2, which enables it to significantly reduce the CAPEX of e.g. CO₂ scrubbing equipment by allowing equipment downsizing.

Figure 7 Comparison of published ranges for the effective specific interfacial area a_e . References:

*Jiao et al., 2007*⁶¹; *Munjal et al., 1988*⁵⁴; *Brito, 1992*⁶²; *Mehta and Sharma, 1971*⁶³; *Luo et al., 2012*⁵²; *Mashelkar, 1970*⁶⁴; *Sawant et al., 1979*⁶⁵; *Vidwans and Sharma, 1967*⁶⁶; *Meeuwse et al., 2008*⁶⁷; *Mehta and Sharma, 1970*⁶⁸.

Energy dissipation assessment

A key question that remains is the energetic efficiency of the GLVR in terms of the overall mass transfer efficiency. As the main energy input to the GLVR is the gas flow, the total energy dissipation in the GLVR can be determined by the input power of the gas flow. The total energy dissipation is given by⁶⁹⁻⁷¹:

$$\varepsilon_{total} = \frac{P_{input}}{V_l} \quad (19)$$

where P_{input} is the total input power and V_l is the liquid holdup volume in the GLVR. Following the concept of gas flow being the main energy input to the system, P_{input} is given by:

$$P_{input} = G\Delta P + G\rho_g\left(\frac{1}{2}v_{in}^2 - \frac{1}{2}v_{out}^2\right) \quad (20)$$

where ρ_g is the gas phase density, v_{in} is the superficial gas velocity at the first pressure measuring point and v_{out} is the superficial gas velocity at the exhaust pressure measuring point. As the two pressure measuring points are located at the outer edge and the exhaust (**Figure 3**) respectively, v_{in} and v_{out} can be determined as:

$$v_{in} = \frac{G}{\pi D_R H} \quad (21)$$

$$v_{out} = \frac{G}{\frac{1}{4}\pi D_0^2} \quad (22)$$

Therefore, to calculate the total energy dissipation, obtaining the liquid holdup volume in the GLVR is the key. However, experimentally determining the liquid holdup in such a highly turbulent and dispersed gas-liquid system is a difficult task and it often requires non-invasive visualization techniques and corresponding reactor revamping⁷². A previous study proposed a method to estimate the liquid holdup based on kinetic energy conservation, however, that is only applicable for rather low liquid flow rates²². In this study, a method is proposed to estimate the liquid holdup based on an analogy with fluidized bed pressure drops. The pressure drop in a fluidized bed under fluidization conditions is well-known⁷³:

$$\Delta P = (1 - \varepsilon_f)(\rho_s - \rho_g)gL_f \quad (23)$$

where ε_f is the void fraction, ρ_s is the solid density, ρ_g is the gas density, g is gravity acceleration and L_f is the height of the bed at fluidization condition.

As Eq. 23 describes the balance between the upward gas drag and the weight of the solid particles in a regular fluidized bed in the gravity field, an analogy can be made in the GLVR based on the balance between the radially inward gas drag and the weight of liquid in a centrifugal force field:

$$\Delta P = h_l(\rho_l - \rho_g)aL_t \quad (24)$$

where h_l is the volumetric liquid holdup fraction of the gas-liquid layer, ρ_l is the liquid density, a is the centrifugal acceleration and L_t is the gas-liquid layer thickness as described in Eq. 17. The average centrifugal acceleration a under various operating conditions can be determined by the azimuthal velocity v_r as can be obtained in the previous study ²¹:

$$a = \frac{v_r^2}{r} \quad (25)$$

The liquid holdup volume is finally determined by multiplying the volumetric liquid holdup fraction with gas-liquid layer volume:

$$V_l = h_l\left(\frac{1}{4}\pi D_R^2 - \pi\left(\frac{1}{2}D_R - L_t\right)^2\right)H \quad (26)$$

Combining the above equations, the total energy dissipation can be estimated. Using the above model, the calculated liquid holdup fraction is within the range of 28%-55% for the range of gas and liquid flow rates in this study, which qualitatively agrees well with the experimental observations ²¹.

As the physical meaning of the volumetric mass transfer coefficient k_{LA_e} is the molar mass transfer rate per unit reactor volume per unit driving force concentration difference, it is a proper indicator to evaluate the reactor performance. **Figure 8** shows the k_{LA_e} as a function of total energy dissipation in the GLVR. With increasing the energy input to the system, a higher volumetric mass transfer coefficient is achieved. In general, a higher gas flow rate drives a

higher energy dissipation. For a fixed gas flow rate, increasing the liquid flow rate will also increase energy dissipation and thus the volumetric mass transfer coefficient. However, at fixed gas flow rates of 25 and 35 Nm³/h for example, the increase of the mass transfer coefficient tends to level off when increasing the liquid flow rate (for a fixed gas flow rate the data points with higher energy dissipation correspond to higher liquid flow rates in **Figure 8**), indicating a lower energetic efficiency. Nevertheless, in terms of the overall data points, a quasi-linear relationship between the mass transfer coefficient and energy dissipation can be observed, showing a relatively stable energetic efficiency of the GLVR within the considered operating conditions.

Figure 8 Volumetric mass transfer coefficient as a function of total energy dissipation in the GLVR.

To further compare the energetic efficiency of the GLVR with other reactors, a figure from the work of Meeuwse et al. ⁶⁹ is adapted to compare the volumetric mass transfer coefficient as a function of total energy dissipation for various reactors including the GLVR, as shown in **Figure 9**. The k_{LAe} range for various reactors is shown with their associated energy dissipation range in each rectangle. The GLVR shows the highest k_{LAe} value, which is 1 to 2 order of magnitude higher than the values of conventional equipment such as a bubble column and a stirred tank, and superior to intensified equipment such as a micro packed bed and a spinning disc reactor. Meanwhile, the energy dissipation of the GLVR is one of the highest, but within the energy dissipation range of the rotor-stator spinning disc reactor. Overall, the achieved k_{LAe} and the associated energy dissipation indicate a favorable energetic efficiency of the GLVR. Especially when considering the large throughputs, small footprint and highly efficient way to create a turbulent gas-liquid layer in a strong centrifugal field (without mechanical rotation), it can be stated that the GLVR is expected to be advantageous in achieving process intensification

for many industrial gas-liquid mass transfer applications. In the context of CO₂ capture, the achieved high k_{La_e} value can lead to CAPEX and OPEX reduction with the use of amine based solvents. However, it should be noted that for practical gas-liquid mass transfer applications, the GLVR geometry design should be optimized for each specific application. It is clear that for CO₂ capture the gas residence time and the distribution of gas and liquid play a crucial role. This can be addressed by a validated computational fluid dynamics (CFD) simulation framework using the validation data provided in this work, which will be elaborated on in our future work.

Figure 9 Comparison of volumetric mass transfer coefficient as function of total energy dissipation for various reactors and GLVR, figure adapted from Meeuwse et al.'s work⁶⁹.

Conclusions

The fundamental interphase mass transfer parameters in a gas-liquid vortex reactor (GLVR) are studied and benchmarked using the NaOH-CO₂ chemisorption system and the Danckwerts' model. The effective specific interfacial area in the GLVR varies in the range of 860 to 2750 m²/m³ and is found to increase with increasing gas and liquid flow rates because of the effect of the gas and liquid flow on the bubble size and gas-liquid layer thickness respectively. The liquid-side mass transfer coefficient also increases both with increasing gas and liquid flow rate. The effect of the gas flow rate is more pronounced due to its impact on the turbulent intensity. When comparing the GLVR with other reactors, it is concluded that the gas-liquid contact in the GLVR is capable of generating a larger interfacial area in a relatively smaller volume. The total energy dissipation of the GLVR is determined to be in the range of 10⁵-10⁶ W/m³, contributing to a superior mass transfer efficiency given the range of the volumetric mass transfer coefficient (10⁰-10¹ 1/s). The GLVR is characterized as a reactor with high mass transfer efficiency and high energy dissipation but overall a favorable energetic efficiency is achieved. This fundamental work and assessment confirms that the GLVR has promising

prospects to achieve process intensification in practical gas-liquid applications controlled by the interphase mass transfer such as CO₂ capture.

Nomenclature

A_e	Effective interfacial area, m ²
a_e	Effective specific interfacial area, m ² /m ³
a	Centrifugal acceleration, m/s ²
C_{CO_2}	CO ₂ concentration at the gas-liquid interface, mol/m ³
$\Delta C_{CO_3^{2-}}$	Concentration difference of Na ₂ CO ₃ at the reactor inlet and outlet, mol/m ³
C_{OH}	Liquid bulk concentration of hydroxyl ions, M or mol/m ³
D_{CO_2}	Diffusivity coefficient of CO ₂ in the NaOH solution, m ² /s
D_o	Exhaust diameter, mm
D_R	Reactor diameter, mm
E	Enhancement factor
G	Gas flow rate, Nm ³ /h
g	Gravity acceleration, m/s ²
H	Reactor height, mm
Ha	Hatta number, $Ha = \frac{\sqrt{D_{CO_2} k_1}}{k_L}$
He_{CO_2}	Henry's law volatility constant, Pa·m ³ /mol
h_l	Volumetric liquid holdup fraction
k_1	Pseudo first-order rate constant, 1/s
k_L	Liquid-side mass transfer coefficient, m/s
k_{La_e}	Volumetric liquid-side mass transfer coefficient, 1/s
k_{OH}	Rate constant, m ³ /mol/s
L	Liquid flow rate, kg/h or m ³ /s
L_f	Height of a fluidized bed at fluidization condition, m

L_t	Gas-liquid layer thickness, mm
N_A	Overall absorption rate flux, mol/(m ² ·s)
N_i	Instant absorption rate flux, mol/(m ² ·s)
\dot{n}_{CO_2}	Molar absorption rate, mol/s
P_{CO_2}	Gas bulk CO ₂ partial pressure, Pa
P_{input}	Total input power, W
ΔP	Pressure drop, Pa
R	Gas-liquid volumetric ratio
R_{CO_2}	Volumetric absorption rate, mol/(m ³ ·s)
R_r	Reaction rate, mol/(m ³ ·s)
r	Radius, m
s	Renewal frequency, 1/s
t	Time, s
V_l	Liquid holdup volume, m ³
v_{in}	Superficial gas velocity at the first pressure measuring point, m/s
v_{out}	Superficial gas velocity at the exhaust pressure measuring point, m/s
v_r	Azimuthal velocity, m/s
ε_{total}	Total energy dissipation, W/m ³
ε_f	Void fraction in a fluidized bed
ρ_g	Gas phase density, kg/m ³
ρ_l	Liquid phase density, kg/m ³
ρ_s	Solid phase density, kg/m ³

Acknowledgments

Yi Ouyang gratefully acknowledges financial support from a postdoctoral fellowship from the Research Foundation – Flanders (FWO) grant number 1273421N. We gratefully acknowledge

the financial support of the Flemish Government and Flanders Innovation & Entrepreneurship (VLAIO) through the Moonshot project CAPTIN (HBC.2019.0109). In addition, the research leading to these results received funding from the European Research Council under the European Union's Horizon 2020 research and innovation programme / ERC grant agreement n° 818607

References

1. Abu-Zahra MRM, Niederer JPM, Feron PHM, Versteeg GF. CO₂ capture from power plants. Part II. A parametric study of the economical performance based on monoethanolamine. *Int J Greenh Gas Control*. 2007;1(2):135-142. doi:10.1016/S1750-5836(07)00032-1
2. Wang M, Joel AS, Ramshaw C, Eimer D, Musa NM. Process intensification for post-combustion CO₂ capture with chemical absorption: A critical review. *Appl Energy*. 2015;158:275-291. doi:10.1016/j.apenergy.2015.08.083
3. Rozanska X, Wimmer E, De Meyer F. Quantitative Kinetic Model of CO₂ Absorption in Aqueous Tertiary Amine Solvents. *J Chem Inf Model*. 2021;61(4):1814-1824. doi:10.1021/acs.jcim.0c01386
4. Papadopoulos AI, Tzirakis F, Tsivintzelis I, Seferlis P. Phase-Change Solvents and Processes for Postcombustion CO₂ Capture: A Detailed Review. *Ind Eng Chem Res*. 2019;58(13):5088-5111. doi:10.1021/acs.iecr.8b06279
5. Van Straelen J, Geuzebroek F. The thermodynamic minimum regeneration energy required for post-combustion CO₂ capture. In: *Energy Procedia*. Vol 4. Elsevier Ltd; 2011:1500-1507. doi:10.1016/j.egypro.2011.02.017
6. Baburao B, Bedell S, Restrepo P, et al. Advanced amine process technology operations and results from demonstration facility at EDF Le Havre. In: *Energy Procedia*. Vol 63. Elsevier Ltd; 2014:6173-6187. doi:10.1016/j.egypro.2014.11.649

7. Baltar A, Gómez-Díaz D, Navaza JM, Rumbo A. Absorption and regeneration studies of chemical solvents based on dimethylethanolamine and diethylethanolamine for carbon dioxide capture. *AIChE J.* 2020;66(1):e16770. doi:10.1002/AIC.16770
8. Jennifer Wilcox. *Carbon Capture*. Springer; 2012.
9. Stankiewicz AI, Moulijn JA. Process intensification: transforming chemical engineering. *Chem Eng Prog.* 2000;96(1):22-34.
10. Sheng M, Xie C, Zeng X, et al. Intensification of CO₂ capture using aqueous diethylenetriamine (DETA) solution from simulated flue gas in a rotating packed bed. *Fuel.* 2018;234:1518-1527. doi:10.1016/j.fuel.2018.07.136
11. Lin C-C, Liu W-T, Tan C-S. Removal of carbon dioxide by absorption in a rotating packed bed. *Ind Eng Chem Res.* 2003;42(11):2381-2386.
12. Jassim MS, Rochelle G, Eimer D, Ramshaw C. Carbon dioxide absorption and desorption in aqueous monoethanolamine solutions in a rotating packed bed. *Ind Eng Chem Res.* 2007;46(9):2823-2833. doi:10.1021/ie051104r
13. Liu Y, Yue J, Xu C, Zhao S, Yao C, Chen G. Hydrodynamics and local mass transfer characterization under gas–liquid–liquid slug flow in a rectangular microchannel. *AIChE J.* 2020;66(2):e16805. doi:10.1002/AIC.16805
14. Ganapathy H, Steinmayer S, Shooshtari A, Dessiatoun S, Ohadi MM, Alshehhi M. Process intensification characteristics of a microreactor absorber for enhanced CO₂ capture. *Appl Energy.* 2016;162:416-427. doi:10.1016/j.apenergy.2015.10.010
15. Aghel B, Sahraie S, Heidaryan E, Varmira K. Experimental study of carbon dioxide absorption by mixed aqueous solutions of methyl diethanolamine (MDEA) and piperazine (PZ) in a microreactor. *Process Saf Environ Prot.* 2019;131:152-159. doi:10.1016/j.psep.2019.09.008
16. Yao C, Zhao Y, Zheng J, Zhang Q, Chen G. The effect of liquid viscosity and modeling

- of mass transfer in gas–liquid slug flow in a rectangular microchannel. *AIChE J.* 2020;66(5):e16934. doi:10.1002/AIC.16934
17. Zhao B, Su Y, Cui G. Post-combustion CO₂ capture with ammonia by vortex flow-based multistage spraying: Process intensification and performance characteristics. *Energy.* 2016;102:106-117. doi:10.1016/j.energy.2016.02.056
 18. Miramontes E, Jiang EA, Love LJ, Lai C, Sun X, Tsouris C. Process intensification of CO₂ absorption using a 3D printed intensified packing device. *AIChE J.* 2020;66(8):e16285. doi:10.1002/AIC.16285
 19. Fox RO. *Computational Models for Turbulent Reacting Flows.* Cambridge University Press; 2003.
 20. de Meyer F, Bignaud C. The use of catalysis for faster CO₂ absorption and energy-efficient solvent regeneration: An industry-focused critical review. *Chem Eng J.* 2022;428:131264. doi:10.1016/J.CEJ.2021.131264
 21. Ouyang Y, Nunez Manzano M, Wetzels R, et al. Liquid hydrodynamics in a gas-liquid vortex reactor. *Chem Eng Sci.* 2021;246:116970. doi:10.1016/j.ces.2021.116970
 22. Ouyang Y, Manzano MN, Beirnaert K, Heynderickx GJ, Van Geem KM. Micromixing in a gas-liquid vortex reactor. *AIChE J.* Published online 2021. doi:10.1002/aic.17264
 23. Ashcraft RW, Kovacevic J, Heynderickx GJ, Marin GB. Assessment of a gas-solid vortex reactor for SO₂/NO_x adsorption from flue gas. *Ind Eng Chem Res.* 2013;52(2):861-875. doi:10.1021/ie300399w
 24. Ashcraft RW, Heynderickx GJ, Marin GB. Modeling fast biomass pyrolysis in a gas-solid vortex reactor. *Chem Eng J.* 2012;207-208:195-208. doi:10.1016/j.cej.2012.06.048
 25. Dai S, Chang Z, Chang C, Akhatov JS, Li X. Numerical study on the directly-irradiated vortex reactor for solar CO₂ coal gasification. *Sol Energy.* 2019;188:573-585.

- doi:10.1016/j.solener.2019.06.035
26. Kulkarni SR, Gonzalez-Quiroga A, Nuñez M, et al. An experimental and numerical study of the suppression of jets, counterflow, and backflow in vortex units. *AIChE J.* 2019;65(8):1-13. doi:10.1002/aic.16614
 27. Vandewalle LA, Van de Vijver R, Van Geem KM, Marin GB. The role of mass and heat transfer in the design of novel reactors for oxidative coupling of methane. *Chem Eng Sci.* 2019;198:268-289. doi:10.1016/j.ces.2018.09.022
 28. Vandewalle LA, Marin GB, Van Geem KM. CFD-based assessment of steady-state multiplicity in a gas-solid vortex reactor for oxidative coupling of methane. *Chem Eng Process - Process Intensif.* 2021;165:108434. doi:10.1016/j.cep.2021.108434
 29. Nunez Manzano M, Gonzalez Quiroga A, Perreault P, et al. Biomass fast pyrolysis in an innovative gas-solid vortex reactor: Experimental proof of concept. *J Anal Appl Pyrolysis.* 2021;156:105165. doi:10.1016/j.jaap.2021.105165
 30. Eliaers P, Ranjan Pati J, Dutta S, De Wilde J. Modeling and simulation of biomass drying in vortex chambers. *Chem Eng Sci.* 2015;123:648-664. doi:10.1016/j.ces.2014.11.043
 31. Trujillo WR, De Wilde J. Influence of solids outlets and the gas inlet design on the generation of a gas-solids rotating fluidized bed in a vortex chamber for different types of particles. *Chem Eng Sci.* 2017;173:74-90. doi:10.1016/j.ces.2017.07.031
 32. Pati JR, Dutta S, Eliaers P, et al. Experimental study of paddy drying in a vortex chamber. 2016;34(9):1073-1084. doi:10.1080/07373937.2015.1093498
 33. De Wilde J. *Gas-Solid Fluidized Beds in Vortex Chambers.* Vol 85. Elsevier B.V.; 2014:256-290. doi:10.1016/j.cep.2014.08.013
 34. Chen L, Shanbhogue S, Pannala S, Shtern V, Ghoniem A, West D. A Nonpremixed Annular Jet Vortex Chamber Reactor for Methane Pyrolysis under Oxygen-Enriched

- Conditions. *Ind Eng Chem Res.* 2021;60(19):7443-7453. doi:10.1021/acs.iecr.1c00131
35. Zhang X, Xiong W, Peng L, Wu Y, Hu X. Highly selective absorption separation of H₂S and CO₂ from CH₄ by novel azole-based protic ionic liquids. *AIChE J.* 2020;66(6):e16936. doi:10.1002/AIC.16936
36. Chen Y-S, Liu H-S. Absorption of VOCs in a rotating packed bed. *Ind Eng Chem Res.* 2002;41(6):1583-1588.
37. Hegely L, Roesler J, Alix P, Rouzineau D, Meyer M. Absorption methods for the determination of mass transfer parameters of packing internals: A literature review. *AIChE J.* 2017;63(8):3246-3275. doi:10.1002/aic.15737
38. Sang L, Luo Y, Chu GW, Liu YZ, Liu XZ, Chen JF. Modeling and experimental studies of mass transfer in the cavity zone of a rotating packed bed. *Chem Eng Sci.* Published online 2016. doi:10.1016/j.ces.2016.12.041
39. Jungnickel C, Wojewódka P, Zielińska-Jurek A, Bokotko R. Spinning Fluids Reactor: A new design of a gas – liquid contactor. *Chem Eng Process - Process Intensif.* 2017;116:40-47. doi:10.1016/j.cep.2017.03.005
40. Aferka S, Viva A, Brunazzi E, Marchot P, Crine M, Toye D. Tomographic measurement of liquid hold up and effective interfacial area distributions in a column packed with high performance structured packings. *Chem Eng Sci.* 2011;66(14):3413-3422. doi:10.1016/j.ces.2011.01.022
41. Aferka S, Marchot P, Crine M, Toye D. Interfacial area measurement in a catalytic distillation packing using high energy X-ray CT. *Chem Eng Sci.* 2010;65(1):511-516. doi:10.1016/j.ces.2009.05.048
42. Yang L, Dietrich N, Loubière K, Gourdon C, Hébrard G. Visualization and characterization of gas-liquid mass transfer around a Taylor bubble right after the formation stage in microreactors. *Chem Eng Sci.* 2016;143:364-368.

doi:10.1016/j.ces.2016.01.013

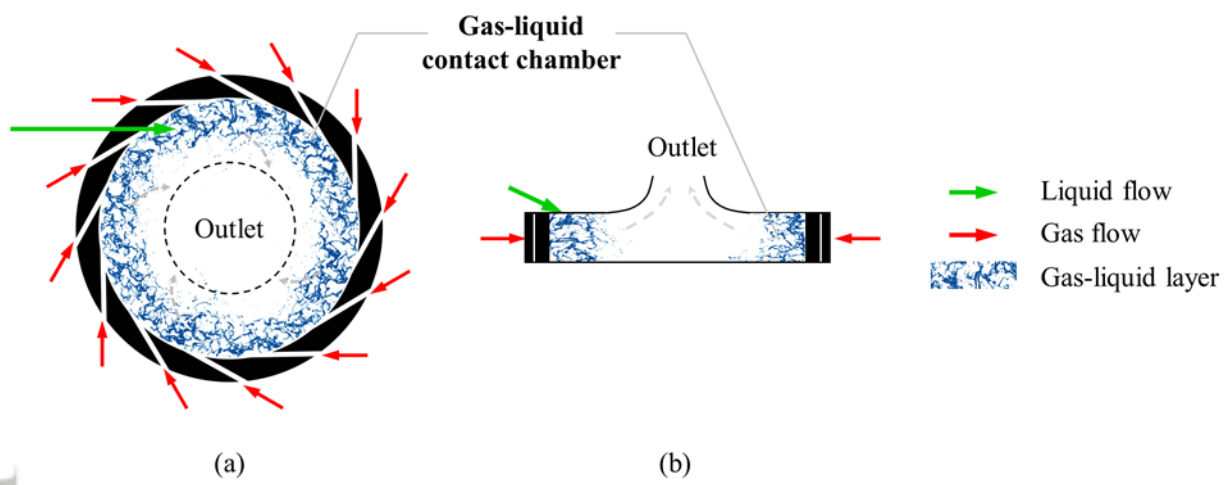
43. Valenz L, Rejl FJ, Šíma J, Linek V. Absorption mass-transfer characteristics of mellapak packings series. *Ind Eng Chem Res.* 2011;50(21):12134-12142. doi:10.1021/ie200577k
44. Danckwerts P V. *Gas-Liquid Reactions.* McGraw-Hill; 1970. <https://iopscience.iop.org/article/10.1149/1.2407312>
45. Sheng M, Xie C, Sun B, et al. Effective Mass Transfer Area Measurement Using a CO₂-NaOH System: Impact of Different Sources of Kinetics Models and Physical Properties. *Ind Eng Chem Res.* 2019;58(25):11082-11092. doi:10.1021/acs.iecr.9b00538
46. Akkarawatkhoosith N, Nopcharoenkul W, Kaewchada A, Jaree A. Mass transfer correlation and optimization of carbon dioxide capture in a microchannel contactor: A case of CO₂-rich gas. *Energies.* 2020;13(20):5465. doi:10.3390/en13205465
47. Luo X, Hartono A, Svendsen HF. Comparative kinetics of carbon dioxide absorption in unloaded aqueous monoethanolamine solutions using wetted wall and string of discs columns. *Chem Eng Sci.* 2012;82:31-43. doi:10.1016/j.ces.2012.07.001
48. Puxty G, Rowland R, Attalla M. Comparison of the rate of CO₂ absorption into aqueous ammonia and monoethanolamine. *Chem Eng Sci.* 2010;65(2):915-922. doi:10.1016/J.CES.2009.09.042
49. Pohorecki R, Moniuk W. Kinetics of reaction between carbon dioxide and hydroxyl ions in aqueous electrolyte solutions. *Chem Eng Sci.* 1988;43(7):1677-1684. doi:10.1016/0009-2509(88)85159-5
50. Yang K, Chu G, Zou H, Sun B, Shao L, Chen JF. Determination of the effective interfacial area in rotating packed bed. *Chem Eng J.* 2011;168(3):1377-1382. doi:10.1016/j.cej.2011.01.100
51. Luo Y, Chu G-WW, Zou H-KK, Zhao Z-QQ, Dudukovic MP, Chen J-F. Gas-liquid effective interfacial area in a rotating packed bed. *Ind Eng Chem Res.*

- 2012;51(50):16320-16325. doi:10.1021/ie302531j
52. Luo Y, Chu G-W, Zou H-K, et al. Mass transfer studies in a rotating packed bed with novel rotors: chemisorption of CO₂. *Ind Eng Chem Res.* 2012;51(26):9164–9172. doi:10.1021/ie300466f
53. Juvekar VA, Sharma MM. Chemical methods of the determination of liquid-side mass transfer coefficient and effective interfacial area in gas-liquid contactors. *Chem Eng Sci.* 1973;28(3):976-978. doi:10.1016/0009-2509(77)80035-3
54. Munjal S, Duduković MP, Ramachandran P. Mass-transfer in rotating packed beds-II. Experimental results and comparison with theory and gravity flow. *Chem Eng Sci.* 1989;44(10):2257-2268. doi:10.1016/0009-2509(89)85160-7
55. Li W-LL, Wang J-HH, Lu Y-CC, Shao L, Chu G-WW, Xiang Y. CFD analysis of CO₂ absorption in a microporous tube-in-tube microchannel reactor with a novel gas-liquid mass transfer model. *Int J Heat Mass Transf.* 2020;150:119389. doi:10.1016/j.ijheatmasstransfer.2020.119389
56. Yoo M, Han S-J, Wee J-H. Carbon dioxide capture capacity of sodium hydroxide aqueous solution. *J Environ Manage.* 2012;114. doi:10.1016/j.jenvman.2012.10.061
57. Van Eckveld AC, Van Der Ham L V., Geers LFG, Van Den Broeke LJP, Boersma BJ, Goetheer ELV. Online monitoring of the solvent and absorbed acid gas concentration in a CO₂ capture process using monoethanolamine. *Ind Eng Chem Res.* 2014;53(13):5515-5523. doi:10.1021/ie402310n
58. Bayliss LE. A Conductivity Method for the Determination of Carbon Dioxide. *Biochem J.* 1927;21(3):662-664. doi:10.1042/bj0210662
59. Pantzali MN, Kovacevic JZ, Heynderickx GJ, Marin GB, Shtern VN. Radial pressure profiles in a cold-flow gas-solid vortex reactor. *AIChE J.* 2015;61(12):4114-4125. doi:10.1002/aic.14912

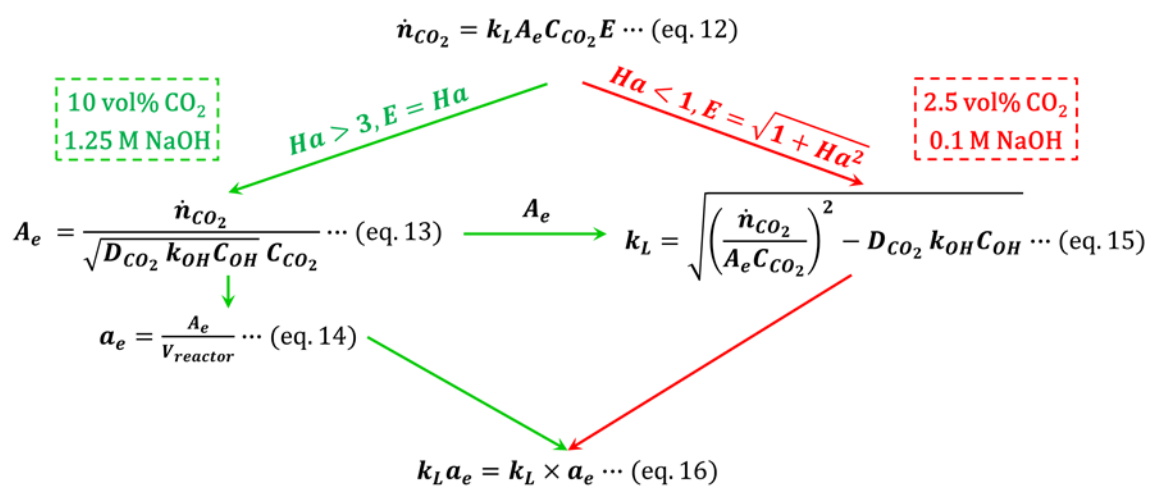
60. Lamont JC, Scott DS. An eddy cell model of mass transfer into the surface of a turbulent liquid. *AIChE J.* 1970;16(4):513-519. doi:10.1002/aic.690160403
61. Jiao W, Liu Y, Qi G, Wang J. Effective interfacial area of high gravity rotating packed bed. 2007;23:296-301+369.
62. Brito MH de. Gas absorption experiments in a pilot plant column with the sulzer structured packing mellapack. Published online 1992:238. doi:10.5075/epfl-thesis-984
63. Mehta VD, Sharma MM. Mass transfer in mechanically agitated gas-liquid contactors. *Chem Eng Sci.* 1971;26(3):461.
64. Mashelkar RA. Bubble columns. *Br Chem Eng.* 1970;10:1297.
65. Sawant SB, Pangarkar VG, Joshi JB. Gas hold-up and mass transfer characteristics of packed bubble columns. *Chem Eng J.* 1979;18(1):143-149. doi:10.1016/0300-9467(79)80024-6
66. Vidwans AD, Sharma MM. Gas-side mass transfer coefficient in packed columns. *Chem Eng Sci.* 1967;22(4):673-684. doi:10.1016/0009-2509(67)80051-4
67. Meeuwse M, van der Schaaf J, Kuster BFM, Schouten JC. Gas-liquid mass transfer in a rotor-stator spinning disc reactor. *Chem Eng Sci.* 2008;65(1):466-471. doi:10.1016/j.ces.2009.06.006
68. Mehta KC, Sharma MM. Mass transfer in spray columns. *Br Chem Eng.* 1970;15(11):1440-1444.
69. Meeuwse M, van der Schaaf J, Schouten JC. Multistage rotor-stator spinning disc reactor. *AIChE J.* 2012;58(1):247-255. doi:10.1002/aic.12586
70. Stemmet CP, Meeuwse M, van der Schaaf J, Kuster BFM, Schouten JC. Gas-liquid mass transfer and axial dispersion in solid foam packings. *Chem Eng Sci.* 2007;62(18-20):5444-5450. doi:10.1016/j.ces.2007.02.016
71. Tschentscher R, Nijhuis TA, van der Schaaf J, Kuster BFM, Schouten JC. Gas-liquid

mass transfer in rotating solid foam reactors. *Chem Eng Sci.* 2010;65(1):472-479.
doi:10.1016/j.ces.2009.05.047

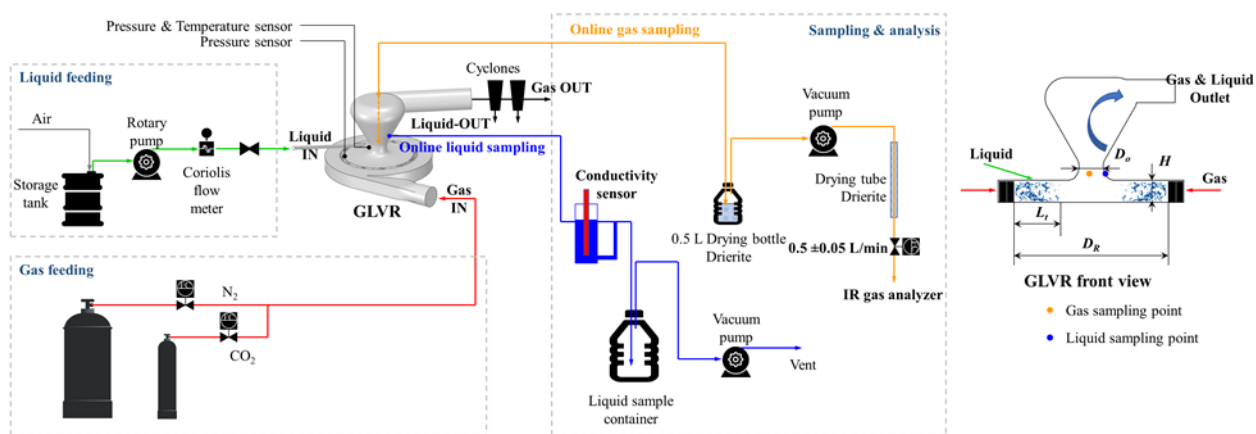
72. Nouri L, Abouda L, Legrand J. Estimation of the micromixing time in the torus reactor by the application of the incorporation model. *Chem Eng Process Process Intensif.* 2014;78:37-43. doi:10.1016/j.cep.2014.02.004
73. Kunii D, Levenspiel O. *Fluidization Engineering*. 2nd editio. Butterworth-Heinemann; 1991.



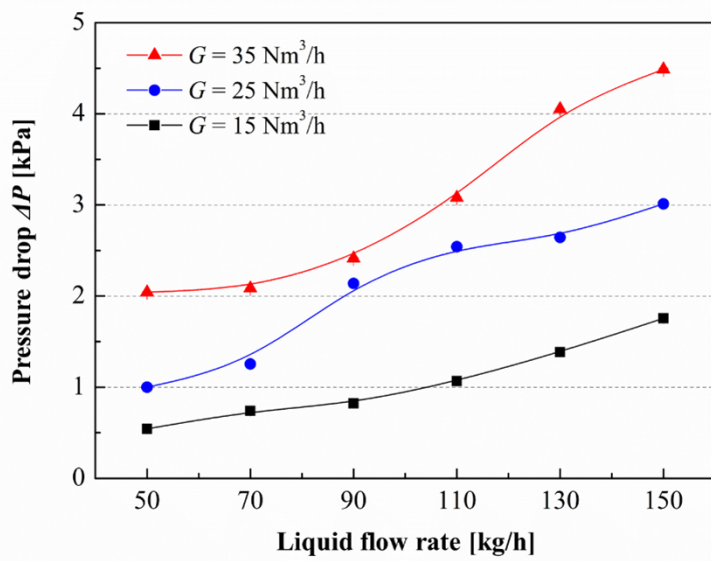
AIC_17608_Figure1.tif



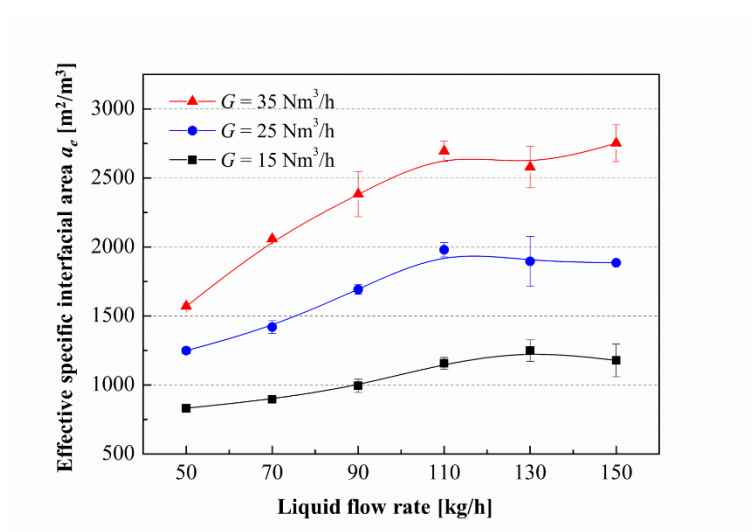
AIC_17608_Figure2.tif



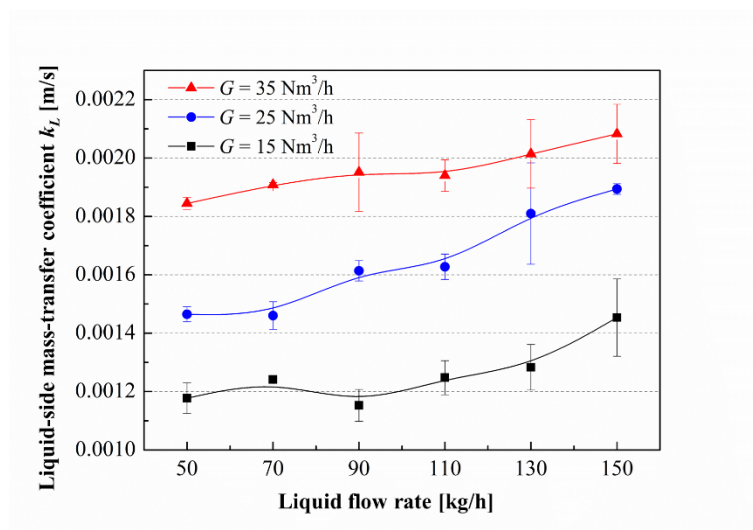
AIC_17608_Figure3.tif



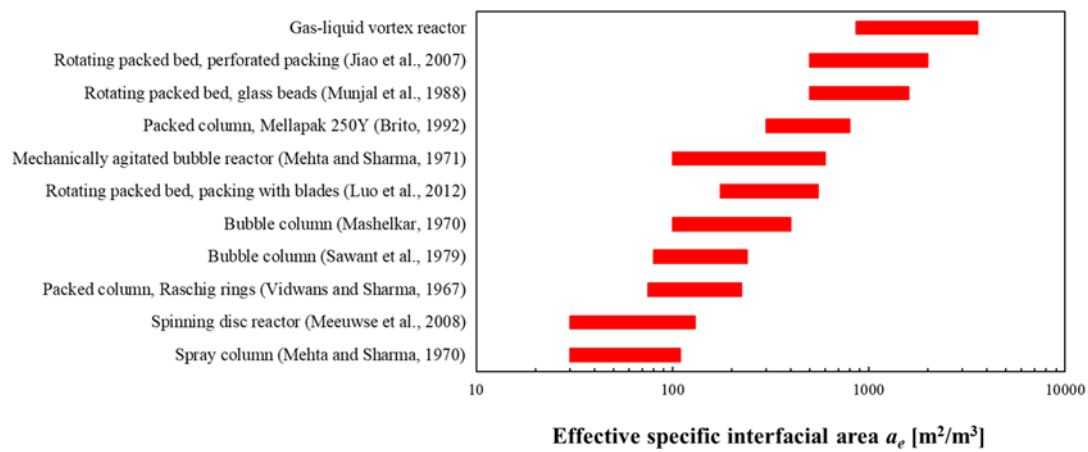
AIC_17608_Figure4.tif



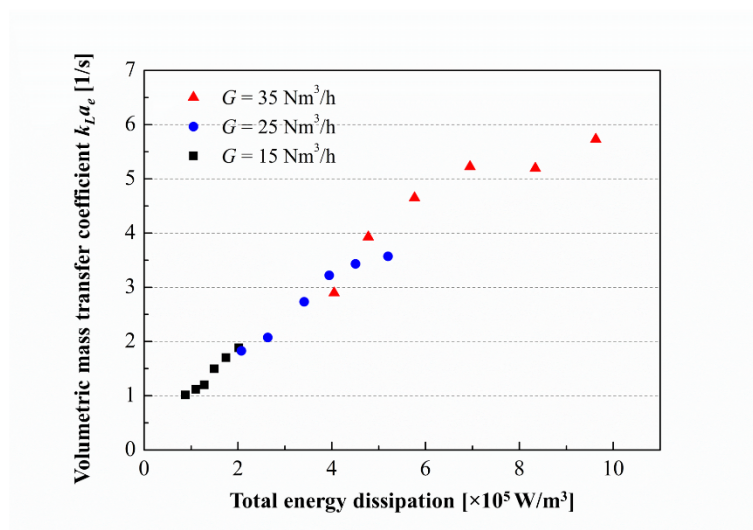
AIC_17608_Figure5.tif



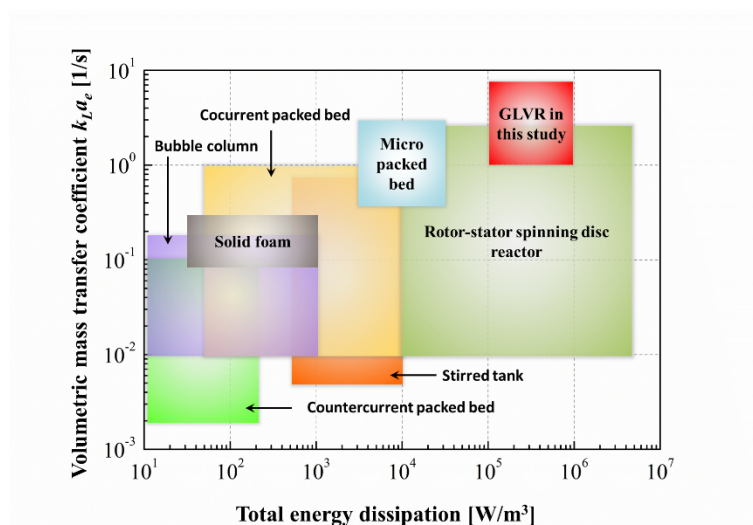
AIC_17608_Figure6.tif



AIC_17608_Figure7.tif



AIC_17608_Figure8.tif



AIC_17608_Figure9.tif

List of Figure Captions

Figure 1 Schematic of the gas-liquid vortex reactor: (a) top view, (b) side view ²²

Figure 2 Schematic overview of the models to determine effective specific interfacial area a_e , liquid-side mass transfer coefficient k_L , and volumetric liquid-side mass transfer coefficient $k_L a_e$.

Figure 3 Schematic view of the gas-liquid vortex reactor setup for the NaOH-CO₂ chemisorption experiments.

Figure 4 Pressure drop over gas-liquid layer in the GLVR for various gas and liquid flow rates.

Figure 5 Effective specific interfacial area in the GLVR for various gas and liquid flow rates.

Figure 6 Liquid-side mass transfer coefficient in the GLVR for various gas flow and liquid flow rates.

Figure 7 Comparison of published ranges for the effective specific interfacial area a_e . References: Jiao et al., 2007 ⁶¹; Munjal et al., 1988 ⁵⁴; Brito, 1992 ⁶²; Mehta and Sharma, 1971 ⁶³; Luo et al., 2012 ⁵²; Mashelkar, 1970 ⁶⁴; Sawant et al., 1979 ⁶⁵; Vidwans and Sharma, 1967 ⁶⁶; Meeuwse et al., 2008 ⁶⁷; Mehta and Sharma, 1970 ⁶⁸.

Figure 8 Volumetric mass transfer coefficient as a function of total energy dissipation in the GLVR.

Figure 9 Comparison of volumetric mass transfer coefficient as function of total energy dissipation for various reactors and GLVR, figure adapted from Meeuwse et al.'s work ⁶⁹.

Table 1 Geometrical parameters of the GLVR.

Parameter	Value
Reactor diameter D_R (mm)	80
Reactor height H (mm)	15
Exhaust diameter D_o (mm)	20
Number of gas inlet slot	12
Slot width (mm)	0.65
Slot angle ($^\circ$)	10
Liquid inlet diameter (mm)	4
Liquid inlet angle ($^\circ$)	18